

Decentralizing Test-time Adaptation under Heterogeneous Data Streams

Zixian Su^{1,2*}, Jingwei Guo^{3*}, Xi Yang^{2†}, Qiufeng Wang², Kaizhu Huang^{4†}

¹University of Liverpool, ²Xi'an Jiaotong-Liverpool University, ³Alibaba Group, ⁴Duke Kunshan University

Homepage: kiwi12138.github.io, jingweio.github.io

Abstract

While Test-Time Adaptation (TTA) has shown promise in addressing distribution shifts between training and testing data, its effectiveness diminishes with heterogeneous data streams due to uniform target estimation. As previous attempts merely stabilize model fine-tuning over time to handle continually changing environments, they fundamentally assume a homogeneous target domain at any moment, leaving the intrinsic real-world data heterogeneity unresolved. This paper delves into TTA under heterogeneous data streams, moving beyond current model-centric limitations. By revisiting TTA from a data-centric perspective, we discover that decomposing samples into Fourier space facilitates an accurate data separation across different frequency levels. Drawing from this insight, we propose a novel Frequency-based Decentralized Adaptation (FreDA) framework, which transitions data from globally heterogeneous to locally homogeneous in Fourier space and employs decentralized adaptation to manage diverse distribution shifts. Interestingly, we devise a novel Fourier-based augmentation strategy to assist in decentralizing adaptation, which individually enhances sample quality for capturing each type of distribution shifts. Extensive experiments across various settings (corrupted, natural, and medical environments) demonstrate the superiority of our proposed framework over the state-of-the-arts.

1. Introduction

Deep learning models often suffer significant performance degradation when deployed in environments where the data distribution differs from that of the training set – a challenge known as domain shift [7, 20]. Recently, Test-Time Adaptation (TTA) [2, 17, 26–28, 31, 34, 36] has emerged as a promising solution by refining model parameters to better align with the encountered data at inference time. It leverages the incoming data stream for real-time adjustments without the need for retraining on a labeled dataset,

*Equal contribution.

†Corresponding author.

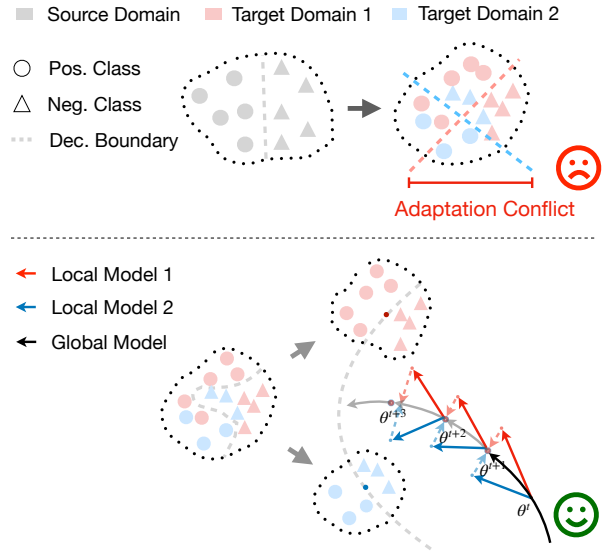
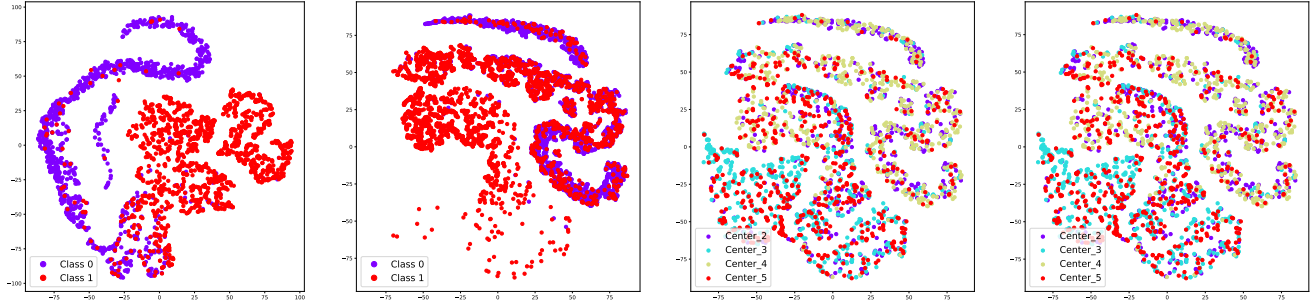


Figure 1. Decentralized adaptation overcomes the conflict within heterogeneous data streams by enabling multiple local model optimizations towards a simplified class decision boundary.

enabling swift model adaptation to unpredictable data characteristics during deployment.

Despite their success, the effectiveness of current TTA models is generally constrained within ideal testing conditions – often involving homogeneous test samples with similar types of distribution shifts. While attempts have been made to address dynamic target distributions in continually changing environments [36], they fundamentally presume a uniform target domain at any time point. Their focus remains on enhancing model robustness against regular changes by stabilizing the fine-tuning process either by periodically resetting model weights [27, 28] or by down-weighting samples that deviate from the estimated distribution [17, 26]. Although these model-centric approaches may offer temporary relief, they do not fully recognize the intrinsic heterogeneity of real-world data. In practice, distribution shifts do not necessarily occur gradually over time but can be multifaceted at a single moment, involving heterogeneous and even conflicting shifts that current TTA



(a) Features produced by adapting models on single type of distribution shift where two classes are mostly separated. (b) Features produced by adapting models on multiple types of distribution shift where two classes are largely overlapped. (c) Features extracted by pretrained models from different centers are completely indistinguishable from one another. (d) High-frequency information of images from four different centers facilitates clear and distinct separation among them.

Figure 2. t-SNE visualizations of the Camelyon17 dataset [1], including pathology slide images from five centers (domains), where the model is pretrained on C1 and tested on C2-C5. (a-b) Features from C4 are presented as an example to illustrate the distinction in model adaptation when addressing single vs multiple distribution shifts. (c-d) Comparison of features extracted by pretrained models and high-frequency information from images across four different domains. Sample features are obtained prior to the final classification layer.

models fail to adequately capture.

To address this, it is crucial to understand how these heterogeneous distribution shifts impact model adaptation. When a model attempts to adjust simultaneously to multiple diverse and potentially conflicting shifts, it may encounter adaptation conflicts. Specifically, adjustments made to accommodate one type of shift can interfere with adaptations for another, as different shifts may require conflicting changes to the model parameters. For instance, adapting to variations in image brightness might necessitate parameter updates that conflict with those needed for texture changes. Such conflicts prevent models from generalizing effectively across all encountered shifts, leading to irreversible degradation in predictive capabilities.

Recognizing these issues, we argue for *shifting from a model-centric to a data-centric approach that proactively addresses distribution diversity in Fourier space*. The rationale is that the frequency domain, unlike the common spatial domain, enables a clearer separation of data variations across different frequency levels. For example, high-frequency components are typically associated with fine-grained features like edges and textures, whereas low-frequency components generally relate to overall structural patterns such as shapes and illumination. By decomposing data into these frequency components, we can effectively isolate and manage different types of distribution shifts. Moreover, since the Fourier transform operates directly on the raw input images at the pixel level, it does not depend on pretrained model outputs, avoiding potential uncertainties due to significant distribution shifts. Importantly, this proactive separation allows us to manage distribution diversity prior to adaptation, offering a robust foundation for subsequent model enhancement.

Building on this insight, we propose a Frequency-based

Decentralized Adaptation (FreDA) framework. Specifically, we first dynamically partition incoming data in the Fourier domain using high-frequency information. This initial segmentation facilitates the transition from globally heterogeneous to locally homogeneous data subsets before any model adaptation occurs. On this basis, we propose a decentralized learning strategy that allows multiple local models to independently adjust to their specific data segments while periodically exchanging knowledge to form a cohesive global model. This dual approach not only captures the diversity of distribution shifts to reduce potential conflicting adaptations but also leverages periodic communication among local models to enhance the global model’s generalization across multiple shifts. Furthermore, we introduce a Fourier-based augmentation mechanism paired with an entropy-based sampling strategy, which significantly increases both the quantity and quality of samples for each type of shift. This enhancement further improves the model’s robustness and predictive capabilities in dynamic environments. To summarize, the main contributions of this work are three-fold:

- We identify that many existing TTA methods are restricted in a *model-centric* paradigm that overlooks the data heterogeneity inherent in real-world scenarios. This oversight results in ineffective adaptation when facing diverse distribution shifts simultaneously.
- We revisit TTA from a *data-centric* perspective and introduce the FreDA framework. It reinterprets principles from both Fourier space and decentralized learning, leveraging specialized local adaptations to manage heterogeneous distribution shifts at test time.
- We conduct extensive evaluations across corrupted, natural, and medical scenarios – demonstrating its consistent superiority under various circumstances.

2. Preliminaries

Test-Time Adaptation under Mixed Distributions. Test-time adaptation (TTA) aims to adjust a model $q_\theta(y|x)$, initially trained on a source dataset $\mathcal{D}_s = \{(x, y) \sim p_s(x, y)\}$, to a target domain $\mathcal{D}_t = \{(x, y) \sim p_t(x, y)\}$ without access to source data or target labels. Traditionally, TTA handles covariate shift by assuming $p_s(y|x) = p_t(y|x)$ while $p_s(x) \neq p_t(x)$. This challenge intensifies when \mathcal{D}_t includes multiple non-i.i.d sub-distributions $p_{t_i}(x)$, complicating the adaptation process:

$$p_t(x) \rightarrow \{p_{t_1}(x), p_{t_2}(x), \dots, p_{t_N}(x)\}.$$

Specifically, we have $\mathcal{D}_t = \mathcal{D}_{t_1} \cup \mathcal{D}_{t_2} \cup \dots \cup \mathcal{D}_{t_N}$ where $x \in \mathcal{D}_{t_1}$ satisfying $x \sim p_{t_1}(x)$. This scenario requires the model $q_\theta(y|x)$ to effectively handle the heterogeneous and evolving target distribution to maintain robust performance. TTA strategies must therefore refine the model to optimize its predictive accuracy across these diverse sub-domains, ensuring consistent and reliable performance amidst significant distributional variability.

Fourier Transformation. Analyzing the frequency components of images is essential for understanding their underlying structures, and Fourier transformation plays a central role in this process. For a single-channel image x , its Fourier transformation $F(x)$ is given by: $F(x)(u, v) = \sum_{h=0}^{H-1} \sum_{w=0}^{W-1} x(h, w) e^{-j2\pi(\frac{h}{H}u + \frac{w}{W}v)}$ where H and W denote the height and width of the image, respectively, and u and v are the frequency coordinates. The inverse Fourier transformation $F^{-1}(x)$ allows for reconstructing the original image from its frequency spectrum, efficiently computed using the Fast Fourier Transform (FFT). In the frequency domain, images are characterized by amplitude $A(x)$ and phase $P(x)$ components, derived from the real $R(x)$ and imaginary $I(x)$ parts of $F(x)$:

$$\begin{aligned} A(x)(u, v) &= \sqrt{R^2(x)(u, v) + I^2(x)(u, v)}, \\ P(x)(u, v) &= \arctan\left(\frac{I(x)(u, v)}{R(x)(u, v)}\right), \end{aligned} \quad (1)$$

where $A(x)$ reveals the intensity of the frequency content, e.g., high-frequency amplitudes highlight edges and fine details while low-frequency amplitudes emphasize the overall structure and gradual changes, and $P(x)$ encodes the position of these features within the spatial domain.

3. Connections to Previous Studies

3.1. Non-i.i.d. in Test-time Adaptation

The non-i.i.d. problem in Test-Time Adaptation (TTA) challenges the conventional assumption that target batches are independent and identically distributed (i.i.d.), pushing the boundaries of TTA in real-world scenarios. This issue can be decomposed into two distinct challenges:

Dependent Sampling. This problem arises when the sampling within the target stream is dependent at the class level. Existing methods [9, 22, 32, 45, 47, 48] have addressed this by aiming for class-balanced datasets during model updates, mitigating risks associated with class imbalance over time. They typically adjust sample proportions based on pseudo labels or extend data collection periods to reduce dependent sampling. However, unlike these methods that concentrate on mitigating class-level imbalances, our work focuses on enhancing TTA models in the presence of diverse sample styles or mixed distributions. We address data heterogeneity at the sample level, aiming to improve model adaptation capabilities in face of varying distribution shifts that are not captured by class balancing techniques. Notably, although our method is not tailored for class-dependent issues, our experimental results demonstrate that when class-dependent and mixed distributions coexist, our approach still achieves the best performance – showcasing the broad applicability of our model design.

Mixed Distributions. While attempts have been made to address dynamic target distributions in continually changing environments [17, 26, 28, 36, 45], they fundamentally assume a uniform target domain at each time point. Their approach focuses on strengthening model adaptation to constant changes by stabilizing the fine-tuning process, using periodic model parameter resets [27, 28] or down-weighting samples that deviate from model expectation [17, 26, 28]. These *model-centric* approaches fail to capture the actual data heterogeneity encountered in practice, causing model degradation in real-world deployment. In contrast, our work re-examines this problem from a *data-centric* perspective. We manage heterogeneous data streams by decomposing samples into the frequency domain, which facilitates an accurate data separation and allows us to address distribution diversity before adaptation occurs. Although a recent work [27] also consider mixed distribution scenarios, their study targets a broader ‘‘Dynamic Wild World’’ topic without delving deeply into this data heterogeneity problem. Conversely, our study focuses on investigating and managing heterogeneous data streams in TTA and proposing tailored strategies to address this problem.

3.2. Multi-Target Domain Adaptation

Test-time Adaptation under mixed distribution resembles the multi-target unsupervised domain adaptation (MT-UDA) setting [6, 8, 15, 19], where multiple domains exist within the target domain. However, TTA introduces complexities that far exceed those in conventional MT-UDA settings, primarily due to: **1) Inaccessible Labeled Source Data** – In TTA, the labeled source distribution is not available, making it challenging to leverage source-target dissimilarities directly. **2) Dynamic and Unpredictable Target Streams** – TTA operates on a continuous influx of data, potentially

incorporating new, unforeseen distributions, rather than a static, fully observable target dataset. This continuous nature of data flow prevents the establishment of a comprehensive understanding of the target distribution. These constraints complicate the formulation of adaptation strategies that depend on discerning the differences between various subdomains within the target.

3.3. Decentralized learning, federated learning, and distributed learning

This work also intersects with decentralized, federated, and distributed learning due to our approach of splitting data batches into disjoint subsets and applying decentralized model adaptation: **1)** Decentralized learning typically focuses on learning from decentralized, non-i.i.d. data [13]. In this work, however, the data is not originally decentralized; all target samples arrive together, while we proactively split them into disjoint subsets, revealing latent non-i.i.d. characteristics and enabling the effective use of decentralized learning techniques. **2)** Federated learning considers data privacy and multi-institutional collaborations within decentralized learning [24]. In our case, as target samples are mixed in a batch, data privacy is not a constraint. However, like federated learning, our approach also involves model collaboration where multiple local models periodically share insights to form a cohesive global model. **3)** Distributed learning aims to improve training efficiency on large-scale datasets by partitioning data for synchronized training [23]. In contrast, our method operates in a real-time fine-tuning context with limited data at one time, hence scalability is less of a concern.

3.4. Frequency Domain Learning

In recent years, frequency-based techniques have become integral to transfer learning strategies. For domain generalization, extensive studies apply frequency analysis to gain insights into the learning behavior and model robustness of DNNs [35, 40, 41, 44]. Some approaches leverage data augmentation to improve model performance. They implement adversarial training to identify the most impactful augmentations [18, 21] or introducing generated Fourier-basis functions as additive noise [30, 33] complementary to visual augmentations. In domain adaptation, researchers implement data augmentation processes involving linear interpolation between the amplitude spectra of images with different styles [38, 39, 42, 43]. This methodology effectively reduces domain discrepancies and mitigates the risk of over-fitting to low-level statistical details inherent in amplitude information.

Motivated by these advancements, we observe that frequency information is a potent domain characteristic. This realization, combined with the insight that augmentations to the amplitude component can mitigate overfitting, par-

ticularly due to the uniform amplitude distributions resulting from prior clustering, forms the core inspiration for our FreDA approach. While our proposed frequency-domain perturbation strategy shares the underlying idea of manipulating the amplitude component with these prior works, we distinguish ourselves by introducing subtle perturbations directly to the original amplitude components of carefully selected samples. This strategy is better suited to unsupervised fine-tuning task, where the TTA process is sensitive, and excessive augmentation may cause model degradation.

4. TTA under Mixed Distribution Shifts: A Fourier Perspective

4.1. Motivations

Test-Time Adaptation (TTA) methods have been instrumental in managing domain shifts under a single type of target distribution. However, their effectiveness significantly diminishes under scenarios involving multiple distribution shifts. This is evident as models exhibit a marked decrease in sample class discriminability on the same dataset when exposed to mixed target distributions, as demonstrated by comparing Figure 2(a) and (b). A direct approach to addressing this issue involves segregating samples belonging to different target distributions. However, in real-time applications, the specific target subdomains from which incoming samples originate, or whether they conform to the same distribution shifts, are generally agnostic. Attempting to cluster samples based on features extracted by the model can be misleading, as samples from different distributions may exhibit similarities due to belonging to the same category, resulting in poor separability of different target subdomains as shown in Figure 2(c). Interestingly, when clustering is based directly on the high-frequency information of the samples – without relying on model-derived feature extractors – a significant distinction can be made between samples from different target distributions, as shown in Figure 2(d). This observation is not unexpected, considering high-frequency information typically captures variations in image textures and styles, focusing more on the underlying differences in data distributions. Building on the experimental observations and analysis outlined above, the following section proposes leveraging the frequency domain for enhancing the adaptability of TTA methods in more realistic settings involving mixed distribution shifts.

4.2. Frequency-based Decentralized Adaptation

The previous discussions highlight how heterogeneity within target distribution can hinder model adaptation. This raises a natural question: *How can we manage this distributional heterogeneity to achieve better adaptation?* As established in our earlier section, effectively distinguishing samples associated with different distribution shifts is vital

for successful domain adaptation. Moreover, the similarity in high-frequency information of samples provides a strong indication of whether they belong to the same or different target distributions.

Building upon these findings, we tackle the TTA problem by capitalizing on the high-frequency data components and propose a novel Frequency-based Decentralized Adaptation (FreDA) framework. It employs a data-centric approach to partition target samples into multiple homogeneous subdomains in Fourier space, enabling an accurate model adaptation. This strategy is complemented by a novel frequency-based augmentation technique that enriches each target subdomain with augmented samples, thereby further bolstering model adaptation. The overall pipeline of FreDA is detailed in Algorithm 1.

4.2.1. Frequency-based Decentralized learning

Insight: Fourier transform offers an effective method to extract different frequency components from images, with high-frequency information particularly useful for capturing fine-grained details such as texture and noise. These details often highlight subtle variations among different distribution shifts. By harnessing high-frequency components from images, we can distinguish samples that lead to different distribution shifts within a TTA setting through a simple clustering technique.

Solution: Based on this intuitive insight, we propose a new module called Frequency-based Decentralized Learning. This module leverages frequency information directly extracted from the pixel space to systematically partition data into multiple homogeneous subsets, enabling multiple local models to specialize in capturing each distribution shift individually (see Figure 1). Concurrently, our method enhances collaborative learning by allowing periodic parameter sharing among these local models, thereby boosting the overall model adaptability to diverse distribution shifts.

Frequency Feature Extraction. We start by extracting frequency domain features from the input images to identify distinct distribution shifts. Let $\mathbf{X} \in \mathbb{R}^{n \times c \times h \times w}$ denote a batch of input images, where n is the batch size, c is the number of channels, h and w are the height and width of the images. We first apply a Fourier transform \mathcal{F} to each image \mathbf{X}_i to obtain its frequency domain representation $\mathcal{F}(\mathbf{X}_i) \in \mathbb{C}^{h \times w \times c}$. Particularly, we focus on the amplitude spectrum $A(x)(u, v)$ in Eq. 1, filtering out low-frequency elements using mask $M(u, v) = \mathbb{1} \left((u < \frac{h}{4} \vee u > \frac{3h}{4}) \vee (v < \frac{w}{4} \vee v > \frac{3w}{4}) \right)$ to emphasize the high-frequency components $G(x)(u, v)$ that are more likely to indicate shifts in distribution:

$$G(x)(u, v) = A(x)(u, v) \cdot M(u, v). \quad (2)$$

Frequency-Based Clustering. We then employ a clustering algorithm (e.g., K-means) to partition the frequency features into K clusters, each corresponding to a different type

of distribution shift. The process is formalized as:

$$\min_{\mathbf{C}, \mathbf{Z}} \sum_{i=1}^n \|\mathbf{A}_{h,f,i} - \mathbf{C}\mathbf{z}_i\|_2^2, \quad (3)$$

where $\mathbf{A}_{h,f,i} = \text{vec}(G(x))$, $\mathbf{C} \in \mathbb{C}^{K \times d}$, $\mathbf{Z} \in \{1, \dots, K\}^n$ denotes the 1D high-frequency component of the amplitude spectrum (the centroids of the clusters and the cluster assignments for each image), hf refers to high-frequency components, and $d = h \times w \times c$ is flattened dimension.

Decentralized Fine-tuning. Test-time fine-tuning is then decentralized across these clusters, allowing for specialized adaptation within each subgroup: For each cluster k , we adapt a specialized model $q_{\theta_k}(y|x)$ that is fine-tuned using only the data within that cluster:

$$\theta_k^* = \arg \min_{\theta_k} \mathbb{E}_{x \sim p_{t,k}} [\mathcal{L}(q_{\theta_k}(x))], \quad (4)$$

where $p_{t,k}$ represents the data distribution within cluster k , and \mathcal{L} is the loss function.

Parameter Aggregation. To integrate knowledge from all subnetworks and prevent degradation on specific subdomains, we perform an aggregation of their parameters:

$$\theta_{\text{global}} = \sum_{k=1}^K \left(\frac{|\mathcal{D}_k|}{\sum_{j=1}^K |\mathcal{D}_j|} \theta_k \right), \quad (5)$$

where $|\mathcal{D}_k|$ denotes the number of samples in cluster k . This aggregation step combines the parameter updates from each subnetwork proportionally to its cluster size. The updated global parameters θ_{global} are then distributed back to each subnetwork, updating its parameters as follows:

$$\theta_k \leftarrow \theta_{\text{global}}. \quad (6)$$

4.2.2. Frequency-based Augmentation

Insight: Although decentralized learning effectively handles data heterogeneity within the current batch, it may still suffer from inadequate characterization of each distribution shift due to limited batch data, specifically considering the uniform amplitude distributions resulting from prior clustering. Typically, TTA methods attempt to enhance the overall quality of observed target samples via data augmentation. However, traditional augmentations in TTA, borrowed from standard computer vision practices such as rotation, clipping, and mixup, albeit beneficial in scenarios with single distribution shifts, struggle to guarantee targeted fine-tuning under more complex, mixed distribution shift scenarios.

Solution: To overcome these limitations, we propose a frequency-based augmentation strategy tailored for TTA under mixed distribution shifts. Our method specifically perturbs the amplitude components of each sample in Fourier space. This targeted approach allows us to augment

Algorithm 1 Framework of Frequency-based Decentralized Learning and Augmentation

Require: Step t , Input $\mathbf{X} \in \mathbb{R}^{n \times h \times w \times c}$, Pretrained source model q_θ , Initialize Feature Repository $\mathcal{R} \leftarrow \emptyset$, CLUSTER_NUM K , KMEANS_SIZE N , COMM_INTERVAL f ;

Step 1: Extract Frequency Features

- 1: **for** $i = 1$ to n **do**
- 2: $\mathbf{A}_{h,f,i} \leftarrow \text{vec}(\text{G}(\mathbf{X}_i))$ \triangleright Extract high-freq components (Eq. 1, 2)
- 3: **end for**

Step 2: Dynamic Clustering

- 4: $\mathcal{R} \leftarrow \mathcal{R} \cup \{\mathbf{A}_{h,f,i}\}_{i=1}^n$ \triangleright Frequency Information Repository
- 5: $\mathcal{R} \leftarrow \mathcal{R}[(|\mathcal{R}| - N + 1) :]$ \triangleright Keep the last N entries for kmeans clustering
- 6: $(\mathbf{C}_t, \mathbf{Z}) \leftarrow \text{K-means}(\mathcal{R}, K, \mathbf{C}_{t-1})$ \triangleright Obtain Cluster Labels
 $\mathbf{Z} = \{Z_i\}_{i=1}^n$ (Eq. 3)

Step 3: Local Model Training

- 7: **for** cluster $k \in \{1, \dots, K\}$ **do**
- 8: $S_k \leftarrow S_k \cup \{\mathbf{X}_i \mid Z_i = k\}$ \triangleright Gather samples for cluster k
- 9: $S_k \leftarrow S_k[(|S_k| - n + 1) :]$ \triangleright Keep the last batch_size = n entries
- 10: $S'_k \leftarrow \text{select_samples}(S_k)$ \triangleright Select samples (Eq. 7)
- 11: **for** each $\mathbf{X}_i \in S'_k$ **do**
- 12: $\tilde{\mathbf{X}}_i \leftarrow \text{augment}(\mathbf{X}_i)$ \triangleright Augment data (Eq. 9)
- 13: Train($q_{\theta_k}, \mathbf{X}_i, \tilde{\mathbf{X}}_i$) \triangleright Train local model (Eq. 4)
- 14: **end for**
- 15: **end for**

Step 4: Compile Predictions

- 16: $\mathbf{Y} \leftarrow \text{collect_sort}(\{q_{\theta_k}(\mathbf{X})\})$ \triangleright Collect and sort predictions

Step 5: Global Model Communication

- 17: **If** $t \% f == 0$: \triangleright Model Communication with interval f (Eq.5, 6)
- 18: $\theta_{\text{global}} \leftarrow \sum_{k=1}^K w_k \theta_k$
- 19: $\theta_k \leftarrow \theta_{\text{global}}$

samples comprehensively, enhancing data quality for each individual shifting case and boosting mode performance across complex real-world scenarios.

Sample Selection Mechanism. We leverage a criterion derived from the weighted entropy framework used in ETA [26] based on two primary conditions:

$$\text{Cri} = \mathbb{1}[(H(\mathbf{y}_t) < H_0) \wedge (|\cos(\mathbf{y}_t, \bar{\mathbf{y}}_{t-1})| < \epsilon)]. \quad (7)$$

The entropy $H(\mathbf{y}_t)$ measures the uncertainty in the current predictions. The cosine similarity $\cos(\mathbf{y}_t, \bar{\mathbf{y}}_{t-1})$ denotes the deviation between the current sample’s class probabilities \mathbf{y}_t and the aggregated class probabilities $\bar{\mathbf{y}}_{t-1}$. ϵ is the threshold for cosine similarity, and H_0 is the fixed entropy threshold. This ensures that selected samples exhibit significant deviations from previous predictions in class distribution and lower prediction uncertainty.

Frequency-Based Augmentation. The augmentation process involves perturbing the amplitude spectrum. Let $A(\mathbf{F}_i)$ represent the amplitude spectrum of a selected sample \mathbf{X}_i . To generate a perturbed amplitude spectrum $\tilde{A}(\mathbf{F}_i)$, we apply a random Gaussian perturbation:

$$\tilde{A}(\mathbf{F}_i) = (1 + \alpha \cdot \Delta) \cdot A(\mathbf{F}_i), \quad (8)$$

where $\Delta \sim \mathcal{N}(0, \sigma^2)$ is a perturbation matrix sampled from a Gaussian distribution, and α is a scaling factor.

Then, the augmented sample $\tilde{\mathbf{X}}_i$ is reconstructed via the inverse Fourier transform to the perturbed amplitude spectrum, combined with the original phase spectrum $P(\mathbf{F}_i)$:

$$\tilde{\mathbf{X}}_i = \mathcal{F}^{-1} \left(\tilde{A}(\mathbf{F}_i), P(\mathbf{F}_i) \right). \quad (9)$$

Loss Function. The training objective combines the entropy loss of the selected samples with a consistency loss from the augmented samples. The total loss is defined as:

$$\mathcal{L}_{\text{total}} = \frac{1}{n} \sum_{i=1}^n H(\mathbf{y}_i) + \lambda \cdot \frac{1}{n} \sum_{i=1}^n \mathcal{L}_{\text{con}}(\hat{\mathbf{y}}_i, \tilde{\mathbf{y}}_i), \quad (10)$$

where the entropy loss $H(\mathbf{y}_i)$ for the original samples is given by $H(\mathbf{y}_i) = -\sum_{j=1}^C \mathbf{y}_{i,j} \log \mathbf{y}_{i,j}$ with \mathbf{y}_i being the predicted probability over the C classes for the sample \mathbf{X}_i , and the consistency loss $\mathcal{L}_{\text{con}}(\tilde{\mathbf{y}}_i, \hat{\mathbf{y}}_i)$ is defined as the cross-entropy between the prediction $\tilde{\mathbf{y}}_i$ of the augmented sample $\tilde{\mathbf{X}}_i$ and the pseudo-label $\hat{\mathbf{y}}_i$ from the original sample: $\mathcal{L}_{\text{con}}(\hat{\mathbf{y}}_i, \tilde{\mathbf{y}}_i) = -\sum_{j=1}^C \hat{\mathbf{y}}_{i,j} \log \tilde{\mathbf{y}}_{i,j}$.

5. Experiments

Datasets and Experimental Settings. To provide a comprehensive evaluation of TTA deployment, we test models over multiple datasets under three different scenarios:

- **Common Image Corruptions:** We evaluate models on CIFAR-10-C, CIFAR-100-C, and ImageNet-C [11] with 10, 100 and 1000 classes, respectively. These benchmarks are designed to assess the model robustness against various corruptions. Each dataset consists of 15 distinct corruptions across five severity levels, resulting in 150,000 at each severity for CIFAR-10-C/100-C, and 750,000 for ImageNet-C.
- **Natural Domain Shifts:** We extend our evaluation to DomainNet126 [29], which presents natural shifts across four domains (Real, Clipart, Painting, Sketch) encompassing 126 classes, representing a subset of the larger DomainNet dataset.
- **Medical Application:** Models are further evaluated on Camelyon17 [1], comprising over 450,000 histopathological patches from lymph node sections for binary classification of normal and tumor tissue, with data originating from five distinct healthcare centers.

For corruption datasets, the model is pretrained on the clean dataset and the 15 corruptions are randomly mixed as the target distribution. We leverage the highest severity = 5 in all the experiments. In DomainNet126 and Camelyon17, one subdomain is selected as the source, and the others serve as mixed target distributions. More implementation details are provided in Appendix A. All reported results are averaged over runs with fixed seeds (0, 1, and 2).

Adaptation Scenarios. To evaluate models in adapting to heterogeneous data streams, we focus on two primary distribution shift scenarios including:

Table 1. Classification error rate (\downarrow) on CIFAR-10-C, CIFAR-100-C, and ImageNet-C (IN-C) respectively under **Mixed Distribution**.

Baseline & Methods	Gauss.	Shot	Impul.	Defoc.	Glass	Motion	Zoom	Snow	Frost	Fog	Brig.	Contr.	Elast.	Pixel	JPEG	Avg.
CIFAR-10-C (WRN-28)	72.3	65.7	72.9	46.9	54.3	34.8	42.0	25.1	41.3	26.0	9.3	46.7	26.6	58.4	30.3	43.5
TBN	45.5	42.8	59.7	34.2	44.3	29.8	32.0	19.8	21.1	21.5	9.3	27.9	33.1	55.5	30.8	33.8
TENT (ICLR 21')	73.5	70.1	81.4	31.6	60.3	29.6	28.5	30.8	35.3	25.7	13.6	44.2	32.6	70.2	34.9	44.1
ETA (ICML 22')	36.2	33.3	52.3	22.9	38.9	22.4	20.5	19.5	19.7	20.4	11.3	35.4	26.6	38.8	<u>25.1</u>	28.2
AdaContrast (CVPR 22')	36.7	34.3	48.8	18.2	39.1	21.1	<u>17.7</u>	<u>18.6</u>	<u>18.3</u>	<u>16.8</u>	9.0	<u>17.4</u>	27.7	44.8	24.9	<u>26.2</u>
CoTTA (CVPR 22')	38.7	36.0	56.1	36.0	36.8	32.3	31.0	19.9	17.6	27.2	11.7	52.6	30.5	<u>35.8</u>	25.7	32.5
SAR (ICLR 23')	45.5	42.7	59.6	34.1	44.3	29.7	31.9	19.8	21.1	21.5	9.3	27.8	33.0	55.4	30.8	33.8
RoTTA (CVPR 23')	60.0	55.5	70.0	23.8	44.1	<u>20.7</u>	21.3	20.2	22.7	16.0	9.4	22.7	27.0	58.6	29.2	33.4
RDumb (NeurIPS 23')	<u>34.9</u>	<u>32.3</u>	49.4	23.3	<u>38.2</u>	23.3	20.7	19.9	19.3	20.7	11.2	29.3	<u>26.7</u>	41.5	25.2	27.7
DeYO (ICLR 24')	45.8	42.3	65.7	21.3	41.8	25.1	19.5	21.1	19.6	19.2	12.3	21.8	28.5	39.3	28.0	30.1
UnMix-TNS (ICLR 24')	50.0	44.4	<u>44.3</u>	34.4	48.2	32.7	30.0	35.5	35.9	47.5	28.1	38.7	43.9	40.0	43.3	39.8
FreDA (ours)	23.1	22.2	32.2	<u>18.7</u>	41.6	18.8	16.8	17.9	19.9	16.9	9.8	13.2	29.1	35.4	28.6	22.9
CIFAR-100-C (ResNeXt-29)	73.0	68.0	39.4	29.3	54.1	30.8	28.8	39.5	45.8	50.3	29.5	55.1	37.2	74.7	41.2	46.4
TBN	62.7	60.7	43.1	35.5	50.3	35.7	34.4	39.9	51.5	27.5	45.5	42.3	72.8	46.4	45.8	45.8
TENT (ICLR 21')	95.6	95.2	89.2	72.8	82.9	74.4	72.3	78.0	79.7	84.7	71.0	88.5	77.8	96.8	78.7	82.5
ETA (ICML 22')	42.6	40.3	34.1	30.3	<u>42.4</u>	32.0	29.4	<u>35.6</u>	<u>35.8</u>	44.1	30.2	41.8	36.9	38.9	40.9	37.0
AdaContrast (CVPR 22')	54.5	51.5	37.6	30.7	45.4	32.1	30.3	36.9	36.5	45.3	<u>28.0</u>	42.7	38.2	75.4	41.7	41.8
CoTTA (CVPR 22')	54.4	52.7	49.8	36.0	45.8	36.7	33.9	38.9	<u>35.8</u>	52.0	30.4	60.9	40.2	<u>38.0</u>	41.1	43.1
SAR (ICLR 23')	75.8	72.7	41.1	29.2	45.2	<u>31.1</u>	28.9	36.7	<u>37.7</u>	43.9	29.3	41.8	<u>37.1</u>	89.2	42.4	45.5
RoTTA (CVPR 23')	65.0	62.3	39.3	33.4	50.0	34.2	32.6	36.6	36.5	45.0	26.4	41.6	40.6	89.5	48.5	45.4
RDumb (NeurIPS 23')	<u>42.3</u>	<u>40.0</u>	34.1	30.5	<u>42.4</u>	31.9	29.5	35.7	35.9	43.6	30.4	41.9	36.9	38.1	<u>40.5</u>	<u>36.9</u>
DeYO (ICLR 24')	<u>57.2</u>	53.4	38.8	34.7	47.3	37.3	34.1	40.8	40.5	50.6	33.3	45.8	41.5	94.5	45.7	46.4
UnMix-TNS (ICLR 24')	65.8	64.1	46.4	37.5	51.7	36.0	36.4	38.5	39.4	51.1	29.3	42.8	43.2	67.8	49.4	46.6
FreDA (ours)	34.8	34.7	<u>36.6</u>	<u>29.4</u>	41.2	29.9	28.4	33.8	33.7	<u>41.1</u>	29.8	34.9	36.9	37.1	38.7	34.7
IN-C (ResNet-50-BN)	97.8	97.1	98.2	81.7	89.8	85.2	77.9	83.5	77.1	75.9	41.3	94.5	82.5	79.3	68.6	82.0
TBN	92.8	91.1	92.5	87.8	90.2	87.2	82.2	82.2	82.0	79.8	48.0	92.5	83.5	75.6	70.4	82.5
TENT (ICLR 21')	99.2	98.7	99.0	90.5	95.1	90.5	84.6	86.6	84.0	86.5	46.7	98.1	86.1	77.7	72.9	86.4
ETA (ICML 22')	90.7	89.2	90.5	<u>77.0</u>	80.6	<u>74.0</u>	<u>68.9</u>	<u>72.4</u>	<u>70.3</u>	64.6	43.9	93.4	69.2	52.3	55.9	<u>72.9</u>
AdaContrast (CVPR 22')	96.2	95.5	96.2	93.2	96.4	96.3	90.5	92.7	91.9	92.4	50.8	97.0	96.6	89.7	87.1	90.8
CoTTA (CVPR 22')	89.1	<u>86.6</u>	<u>88.5</u>	80.9	87.2	81.1	75.8	73.3	75.2	70.5	41.6	<u>85.0</u>	78.1	65.6	61.6	76.0
SAR (ICLR 23')	98.4	97.3	98.0	84.0	87.3	82.6	77.2	77.5	76.1	72.5	43.1	96.0	78.3	61.8	60.4	79.4
RoTTA (CVPR 23')	89.4	88.6	89.3	83.4	89.1	86.2	80.0	78.9	76.9	74.2	37.4	89.6	79.5	69.0	59.6	78.1
RDumb (NeurIPS 23')	<u>89.0</u>	87.6	88.6	78.1	82.3	75.2	70.1	73.0	71.0	65.1	43.9	92.6	<u>70.7</u>	<u>53.7</u>	<u>56.3</u>	73.1
DeYO (ICLR 24')	99.5	99.2	99.5	89.5	95.0	83.9	78.8	75.0	87.8	79.2	47.3	99.2	92.4	59.0	60.4	83.0
UnMix-TNS (ICLR 24')	91.7	92.8	91.7	92.3	93.4	91.5	84.8	86.3	84.1	85.0	62.0	96.5	88.6	81.7	77.3	86.7
FreDA (ours)	72.4	74.0	71.4	76.5	<u>82.3</u>	72.1	64.1	64.4	64.8	59.1	43.7	79.7	71.0	54.2	58.6	67.2
IN-C (VitBase-LN)	65.8	67.3	65.3	68.8	74.4	64.3	66.6	56.8	45.2	48.6	29.2	81.8	57.1	60.8	50.2	60.2
TENT (ICLR 21')	60.6	60.4	59.6	63.6	67.8	57.1	61.2	55.0	48.8	47.4	28.6	66.7	53.9	50.4	44.4	55.0
ETA (ICML 22')	59.3	57.8	57.9	<u>58.8</u>	62.8	52.5	58.2	51.0	46.4	44.2	28.8	58.3	51.1	46.9	41.9	51.7
AdaContrast (CVPR 22')	64.8	63.4	63.3	72.8	76.6	73.7	74.6	67.7	48.0	89.6	30.2	93.2	60.8	57.3	46.3	65.5
CoTTA (CVPR 22')	89.4	92.0	88.9	93.6	92.6	90.6	86.5	94.9	88.2	86.6	75.8	96.5	85.7	93.5	84.6	89.3
SAR (ICLR 23')	<u>58.9</u>	<u>57.6</u>	<u>57.6</u>	59.4	63.6	53.0	58.5	52.3	47.1	45.4	<u>28.3</u>	61.6	51.4	47.4	42.0	52.3
RoTTA (CVPR 23')	64.4	65.6	63.7	67.6	71.3	59.8	64.1	52.7	<u>43.5</u>	48.6	27.9	78.5	54.3	60.4	50.1	58.2
RDumb (NeurIPS 23')	59.7	58.5	58.5	60.0	64.1	54.0	59.0	52.0	46.7	44.5	28.6	61.2	51.9	48.3	42.6	52.6
DeYO (ICLR 24')	60.0	58.6	58.8	58.8	<u>62.4</u>	61.9	50.9	46.7	51.9	45.2	29.7	<u>55.7</u>	51.6	45.8	42.8	52.1
FreDA (ours)	55.9	53.7	55.0	58.0	57.9	50.9	<u>57.4</u>	45.5	42.9	43.9	29.5	51.7	47.8	41.6	40.7	48.8

Table 2. Classification error rate (\downarrow) on CIFAR-10-C/100-C (C10/C100), and ImageNet-C (IN) using ResNet-50-BN and VitBase-LN under **Mixed Distribution & Dependent Sampling**.

Methods	C10	C100	IN(BN)	IN(LN)
Source	43.5	46.5	<u>82.0</u>	60.2
TBN	79.2	92.3	94.2	-
TENT (ICLR 21')	86.6	98.4	99.5	77.9
ETA (ICML 22')	86.1	96.2	99.7	73.9
AdaContrast (CVPR 22')	69.8	73.2	98.5	94.9
CoTTA (CVPR 22')	82.7	92.8	98.0	92.6
SAR (ICLR 23')	78.8	95.8	98.2	54.0
RoTTA (CVPR 23')	64.6	65.3	89.3	74.2
RDumb (NeurIPS 23')	86.2	98.4	98.1	56.5
DeYO (ICLR 24')	87.0	98.1	99.1	<u>52.0</u>
UnMix-TNS (ICLR 24')	<u>41.9</u>	<u>50.1</u>	84.3	-
FreDA (ours)	23.0	34.7	67.2	48.7

- Mixed Domains: A long test sequence where consecutive test samples may come from different domains.
- Mixed Domains & Dependent Sampling: Extends the mixed distribution framework by introducing sequential, time-correlated data from the same class.

The detailed description of the settings can be found in Appendix E. Moreover, While our primary focus is on mixed domains, we have also included the commonly used continual setting for evaluation in Appendix C.

Baselines. We compare FreDA with 10 models: TBN [25], TENT [34], CoTTA [36], ETA [26], SAR [27], AdaContrast [2], RoTTA [45], RDumb [28], DeYO [17], and UnMix-TNS [32]. See more information in Appendix B.

FreDA consistently improves across different distribution shifts. Our method consistently attains the lowest classification error rates across all evaluated datasets (see Table 1 and 3). Notably, on the Camelyon17 dataset, FreDA reduced the error rate to 27.9%, outperforming the next best method by 5.9%. This significant improvement is particularly notable where other approaches falter if compared with no training (TBN), meaning they struggle to adapt to the complex medical imaging data. By effectively handling high variability and intricate patterns in the data, FreDA maintains superior accuracy and adaptability.

FreDA effectively mitigates both covariate and label

Table 3. Classification error rate (\downarrow) on DomainNet126 and Camelyon17 under **Mixed Distribution**.

Methods	DomainNet126					Camelyon17					
	Real	Painting	Clipart	Sketch	Avg.	C1	C2	C3	C4	C5	Avg.
Source	45.2	41.6	49.5	45.3	45.4	21.6	43.6	52.5	47.4	47.6	42.5
TBN	45.5	39.9	45.9	37.5	42.2	26.5	38.5	31.7	39.4	32.8	33.8
TENT (ICLR 21')	42.2	37.8	44.7	37.5	40.6	44.7	50.5	49.9	49.1	48.6	48.6
ETA (ICML 22')	41.1	37.3	43.4	36.4	39.5	47.4	52.5	47.9	49.9	39.2	47.4
SAR (ICLR 23')	43.2	38.5	44.8	37.0	40.9	26.5	38.5	31.7	39.4	32.8	33.8
DeYO (ICLR 24')	40.9	36.4	43.6	36.9	39.4	50.4	50.3	48.8	51.7	50.5	50.4
FreDA (ours)	40.2	36.1	40.0	33.6	37.5	18.6	24.7	24.8	40.5	30.8	27.9

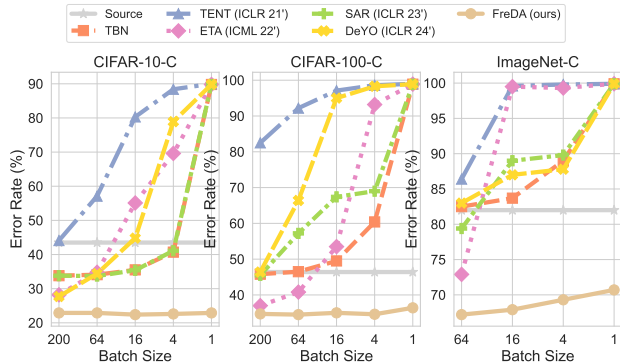


Figure 3. Averaged classification error rate (\downarrow) on CIFAR-10-C/100-C and ImageNet-C using WRN-28, ResNeXt-29 and ResNet-50-BN with various batch size under Mixed Domains.

shifts. In environments characterized by simultaneous covariate and label shifts, our approach keep showing exceptional adaptability (see Table 2). We attribute this success to FreDA’s ability to separate covariate shifts from label shifts via decentralized learning. FreDA achieves this by first isolating target different distribution shifts and then focus on learning label shifts for each specific distribution. This sequential approach prevents models from being overwhelmed by simultaneous shifts, allowing it to address each type of shift independently and effectively.

FreDA remains stable under various batch size. To simulate deployment with constrained batch sizes, we evaluate models under both varying batch sizes and mixed distribution shifts. In Figure 3, we present the results on CIFAR-10-C, CIFAR-100-C, and ImageNet-C datasets using batch sizes ranging from 200 (64) down to 1. Unlike other methods that significantly degrade as batch size decreases – for example the error rate of DeYO increases from 27.7% to 89.8% when batch size drops from 200 to 1 on CIFAR-10-C – FreDA consistently maintains strong performance. This stability under limited batch sizes demonstrates FreDA’s robustness, making it highly suitable for real-world applications where large batches is not always feasible.

FreDA enhances adaptation via synergistic designs. This section validates our designs by ablating its three key mod-

Table 4. Ablation study of FreDA.

DT	SS	SA	C10	C100	IN(BN)	IN(LN)
			44.1	82.5	86.4	55.0
✓			24.8	54.2	81.2	95.2
	✓		29.6	37.5	71.0	51.1
		✓	39.4	71.7	92.9	59.5
✓	✓		24.3	36.3	69.4	49.6
	✓	✓	27.7	36.2	65.9	50.1
✓		✓	24.4	50.2	77.7	95.3
✓	✓	✓	22.9	34.7	67.2	48.8

ules – Decentralized Training (DT), Sample Selection (SS), and Sample Augmentation (SA). The baseline here leverages only the entropy loss. From Table 4, we have the following observations: **1)** Implementing decentralized training alone results in substantial improvements, reducing error rates dramatically across all datasets. **2)** The impact of sample selection varies across datasets. While significantly improving performance on CIFAR100-C, it increase error rate on Camelyon. This variation suggests that sample selection helps the model focus on more representative or challenging samples but may not be effective across all datasets, highlighting its dataset-specific nature. **3)** Sample augmentation alone tends to increase error rates, suggesting that although this approach introduces useful variability, it may introduce unexpected noise under the absence of proper selection or decentralized training. **4)** The combined approach delivers the best performance across all datasets, showing the synergistic effect of our different designs.

6. Conclusion

This paper advances Test-Time Adaptation (TTA) by tackling the real-world complexities of heterogeneous data streams. Our decentralized approach precisely manages diverse data shifts, improving model adaptation in varied settings. By integrating Fourier-based augmentation, we expand the range of confident samples for each distribution shift, further boosting model performance. The experimental results underscore the efficacy of FreDA, highlighting its potential to influence the field and guide future research in adapting to dynamic and diverse data shifts.

References

- [1] Peter Bandi, Oscar Geessink, Quirine Manson, Marcorcy Van Dijk, Maschenka Balkenhol, Meyke Hermsen, Babak Ehteshami Bejnordi, Byungjae Lee, Kyunghyun Paeng, Aoxiao Zhong, et al. From detection of individual metastases to classification of lymph node status at the patient level: the camelyon17 challenge. *IEEE transactions on medical imaging*, 38(2):550–560, 2018. 2, 6
- [2] Dian Chen, Dequan Wang, Trevor Darrell, and Sayna Ebrahimi. Contrastive test-time adaptation. In *Proceedings of the IEEE/CVF Conference on Computer Vision and Pattern Recognition*, pages 295–305, 2022. 1, 7, 11
- [3] Francesco Croce, Maksym Andriushchenko, Vikash Sehwag, Edoardo Debenedetti, Nicolas Flammarion, Mung Chiang, Prateek Mittal, and Matthias Hein. Robustbench: a standardized adversarial robustness benchmark. In *Thirty-fifth Conference on Neural Information Processing Systems Datasets and Benchmarks Track*, 2021. 11
- [4] Mario Döbler, Robert A Marsden, and Bin Yang. Robust mean teacher for continual and gradual test-time adaptation. In *Proceedings of the IEEE/CVF Conference on Computer Vision and Pattern Recognition*, pages 7704–7714, 2023. 11
- [5] Alexey Dosovitskiy. An image is worth 16x16 words: Transformers for image recognition at scale. *arXiv preprint arXiv:2010.11929*, 2020. 11
- [6] Tingliang Feng, Hao Shi, Xueyang Liu, Wei Feng, Liang Wan, Yanlin Zhou, and Di Lin. Open compound domain adaptation with object style compensation for semantic segmentation. *Advances in Neural Information Processing Systems*, 36, 2024. 3
- [7] Yaroslav Ganin and Victor Lempitsky. Unsupervised domain adaptation by backpropagation. In *International Conference on Machine Learning*, pages 1180–1189. PMLR, 2015. 1
- [8] Behnam Gholami, Pritish Sahu, Ognjen Rudovic, Konstantinos Bousmalis, and Vladimir Pavlovic. Unsupervised multi-target domain adaptation: An information theoretic approach. *IEEE Transactions on Image Processing*, 29:3993–4002, 2020. 3
- [9] Taesik Gong, Jongheon Jeong, Taewon Kim, Yewon Kim, Jinwoo Shin, and Sung-Ju Lee. Note: Robust continual test-time adaptation against temporal correlation. *Advances in Neural Information Processing Systems*, 35:27253–27266, 2022. 3
- [10] Kaiming He, Xiangyu Zhang, Shaoqing Ren, and Jian Sun. Deep residual learning for image recognition. In *Proceedings of the IEEE/CVF Conference on Computer Vision and Pattern Recognition*, pages 770–778, 2016. 11
- [11] Dan Hendrycks and Thomas G Dietterich. Benchmarking neural network robustness to common corruptions and surface variations. *arXiv preprint arXiv:1807.01697*, 2018. 6
- [12] Dan Hendrycks, Norman Mu, Ekin Dogus Cubuk, Barret Zoph, Justin Gilmer, and Balaji Lakshminarayanan. Augmix: A simple data processing method to improve robustness and uncertainty. In *International Conference on Learning Representations*, 2020. 11
- [13] Kevin Hsieh, Amar Phanishayee, Onur Mutlu, and Phillip Gibbons. The non-iid data quagmire of decentralized machine learning. In *International Conference on Machine Learning*, pages 4387–4398. PMLR, 2020. 4
- [14] Gao Huang, Zhuang Liu, Laurens Van Der Maaten, and Kilian Q Weinberger. Densely connected convolutional networks. In *Proceedings of the IEEE conference on computer vision and pattern recognition*, pages 4700–4708, 2017. 11
- [15] Takashi Isobe, Xu Jia, Shuaijun Chen, Jianzhong He, Yongjie Shi, Jianzhuang Liu, Huchuan Lu, and Shengjin Wang. Multi-target domain adaptation with collaborative consistency learning. In *Proceedings of the IEEE/CVF conference on computer vision and pattern recognition*, pages 8187–8196, 2021. 3
- [16] Pang Wei Koh, Shiori Sagawa, Henrik Marklund, Sang Michael Xie, Marvin Zhang, Akshay Balsubramani, Weihua Hu, Michihiro Yasunaga, Richard Lanus Phillips, Irena Gao, et al. Wilds: A benchmark of in-the-wild distribution shifts. In *International conference on machine learning*, pages 5637–5664. PMLR, 2021. 11
- [17] Jonghyun Lee, Dahuin Jung, Saehyung Lee, Junsung Park, Juhyeon Shin, Uiwon Hwang, and Sungroh Yoon. Entropy is not enough for test-time adaptation: From the perspective of disentangled factors. In *International Conference on Learning Representations*, 2024. 1, 3, 7, 11
- [18] Chang Liu, Wenzhao Xiang, Yuan He, Hui Xue, Shibao Zheng, and Hang Su. Improving model generalization by on-manifold adversarial augmentation in the frequency domain. *arXiv preprint arXiv:2302.14302*, 2023. 4
- [19] Ziwei Liu, Zhongqi Miao, Xingang Pan, Xiaohang Zhan, Dahua Lin, Stella X Yu, and Boqing Gong. Open compound domain adaptation. In *Proceedings of the IEEE/CVF Conference on Computer Vision and Pattern Recognition*, pages 12406–12415, 2020. 3
- [20] Mingsheng Long, Jianmin Wang, Guiguang Ding, Jianguang Sun, and Philip S Yu. Transfer feature learning with joint distribution adaptation. In *Proceedings of the IEEE International Conference on Computer Vision*, pages 2200–2207, 2013. 1
- [21] Yuyang Long, Qilong Zhang, Boheng Zeng, Lianli Gao, Xianglong Liu, Jian Zhang, and Jingkuan Song. Frequency domain model augmentation for adversarial attack. In *European conference on computer vision*, pages 549–566. Springer, 2022. 4
- [22] Robert A Marsden, Mario Döbler, and Bin Yang. Universal test-time adaptation through weight ensembling, diversity weighting, and prior correction. In *Proceedings of the IEEE/CVF Winter Conference on Applications of Computer Vision*, pages 2555–2565, 2024. 3
- [23] Ryan McDonald, Keith Hall, and Gideon Mann. Distributed training strategies for the structured perceptron. In *Human language technologies: The 2010 annual conference of the North American chapter of the association for computational linguistics*, pages 456–464, 2010. 4
- [24] Brendan McMahan, Eider Moore, Daniel Ramage, Seth Hampson, and Blaise Aguerre y Arcas. Communication-efficient learning of deep networks from decentralized data. In *Artificial intelligence and statistics*, pages 1273–1282. PMLR, 2017. 4

- [25] Zachary Nado, Shreyas Padhy, D Sculley, Alexander D’Amour, Balaji Lakshminarayanan, and Jasper Snoek. Evaluating prediction-time batch normalization for robustness under covariate shift. *arXiv preprint arXiv:2006.10963*, 2020. 7, 11
- [26] Shuaicheng Niu, Jiaxiang Wu, Yifan Zhang, Yafo Chen, Shijian Zheng, Peilin Zhao, and Mingkui Tan. Efficient test-time model adaptation without forgetting. In *International Conference on Machine Learning*, pages 16888–16905. PMLR, 2022. 1, 3, 6, 7, 11
- [27] Shuaicheng Niu, Jiaxiang Wu, Yifan Zhang, Zhiquan Wen, Yafo Chen, Peilin Zhao, and Mingkui Tan. Towards stable test-time adaptation in dynamic wild world. In *International Conference on Learning Representations*, 2023. 1, 3, 7, 11
- [28] Ori Press, Steffen Schneider, Matthias Kümmerer, and Matthias Bethge. Rdumb: A simple approach that questions our progress in continual test-time adaptation. *Advances in Neural Information Processing Systems*, 36, 2024. 1, 3, 7, 11
- [29] Kuniaki Saito, Donghyun Kim, Stan Sclaroff, Trevor Darrell, and Kate Saenko. Semi-supervised domain adaptation via minimax entropy. In *Proceedings of the IEEE/CVF international conference on computer vision*, pages 8050–8058, 2019. 6
- [30] Ryan Soklaski, Michael Yee, and Theodoros Tsiligkaridis. Fourier-based augmentations for improved robustness and uncertainty calibration. *arXiv preprint arXiv:2202.12412*, 2022. 4
- [31] Zixian Su, Jingwei Guo, Kai Yao, Xi Yang, Qiufeng Wang, and Kaizhu Huang. Unraveling batch normalization for realistic test-time adaptation. In *Proceedings of the AAAI Conference on Artificial Intelligence*, pages 15136–15144, 2024. 1
- [32] Devavrat Tomar, Guillaume Vray, Jean-Philippe Thiran, and Behzad Bozorgtabar. Un-mixing test-time normalization statistics: Combatting label temporal correlation. In *International Conference on Learning Representations*, 2024. 3, 7, 11
- [33] Puru Vaish, Shunxin Wang, and Nicola Strisciuglio. Fourier-basis functions to bridge augmentation gap: Rethinking frequency augmentation in image classification. In *Proceedings of the IEEE/CVF Conference on Computer Vision and Pattern Recognition*, pages 17763–17772, 2024. 4
- [34] Dequan Wang, Evan Shelhamer, Shaoteng Liu, Bruno Olshausen, and Trevor Darrell. Tent: Fully test-time adaptation by entropy minimization. In *International Conference on Learning Representations*, 2021. 1, 7, 11
- [35] Haohan Wang, Xindi Wu, Zeyi Huang, and Eric P Xing. High-frequency component helps explain the generalization of convolutional neural networks. In *Proceedings of the IEEE/CVF conference on computer vision and pattern recognition*, pages 8684–8694, 2020. 4
- [36] Qin Wang, Olga Fink, Luc Van Gool, and Dengxin Dai. Continual test-time domain adaptation. In *Proceedings of the IEEE/CVF Conference on Computer Vision and Pattern Recognition*, pages 7201–7211, 2022. 1, 3, 7, 11
- [37] Saining Xie, Ross Girshick, Piotr Dollár, Zhuowen Tu, and Kaiming He. Aggregated residual transformations for deep neural networks. In *Proceedings of the IEEE/CVF Conference on Computer Vision and Pattern Recognition*, pages 1492–1500, 2017. 11
- [38] Qinwei Xu, Ruipeng Zhang, Ya Zhang, Yanfeng Wang, and Qi Tian. A fourier-based framework for domain generalization. In *Proceedings of the IEEE/CVF conference on computer vision and pattern recognition*, pages 14383–14392, 2021. 4
- [39] Qinwei Xu, Ruipeng Zhang, Ziqing Fan, Yanfeng Wang, Yi-Yan Wu, and Ya Zhang. Fourier-based augmentation with applications to domain generalization. *Pattern Recognition*, 139:109474, 2023. 4
- [40] Zhiqin John Xu. Understanding training and generalization in deep learning by fourier analysis. *arXiv preprint arXiv:1808.04295*, 2018. 4
- [41] Zhi-Qin John Xu, Yaoyu Zhang, and Yanyang Xiao. Training behavior of deep neural network in frequency domain. In *Neural Information Processing: 26th International Conference, ICONIP 2019, Sydney, NSW, Australia, December 12–15, 2019, Proceedings, Part I 26*, pages 264–274. Springer, 2019. 4
- [42] Chen Yang, Xiaoqing Guo, Zhen Chen, and Yixuan Yuan. Source free domain adaptation for medical image segmentation with fourier style mining. *Medical Image Analysis*, 79: 102457, 2022. 4
- [43] Yanchao Yang and Stefano Soatto. Fda: Fourier domain adaptation for semantic segmentation. In *Proceedings of the IEEE/CVF conference on computer vision and pattern recognition*, pages 4085–4095, 2020. 4
- [44] Dong Yin, Raphael Gontijo Lopes, Jon Shlens, Ekin Dogus Cubuk, and Justin Gilmer. A fourier perspective on model robustness in computer vision. *Advances in Neural Information Processing Systems*, 32, 2019. 4
- [45] Longhui Yuan, Binhui Xie, and Shuang Li. Robust test-time adaptation in dynamic scenarios. In *Proceedings of the IEEE/CVF Conference on Computer Vision and Pattern Recognition*, pages 15922–15932, 2023. 3, 7, 11
- [46] Sergey Zagoruyko and Nikos Komodakis. Wide residual networks. *arXiv preprint arXiv:1605.07146*, 2016. 11
- [47] Bowen Zhao, Chen Chen, and Shu-Tao Xia. Delta: Degradation-free fully test-time adaptation. In *International Conference on Learning Representations*, 2023. 3
- [48] Zhi Zhou, Lan-Zhe Guo, Lin-Han Jia, Dingchu Zhang, and Yu-Feng Li. Ods: Test-time adaptation in the presence of open-world data shift. In *International Conference on Machine Learning*, pages 42574–42588. PMLR, 2023. 3

Decentralizing Test-time Adaptation under Heterogeneous Data Streams

Supplementary Material

A. Implementation Details

Pretrained Models. We utilize models from RobustBench [3], including WildResNet-28 [46] for CIFAR-10-C and ResNeXt-29 [37] for CIFAR-100-C, both pretrained by Hendrycks et al. [12]. For ImageNet-C, the pretrained ResNet-50 [10] and ViTBase-LN [5] are obtained from torchvision. For DomainNet126, pretrained ResNet-50 are sourced from AdaContrast [2], while for Camelyon17, we train a DenseNet-121 [14] from scratch to 100 epochs with other training specifications outlined in the Wilds benchmark [16].

Hyperparameter Configuration. The batch size is set to 200, 64, 128 and 32 for CIFAR-10/100-C, ImageNet-C, DomainNet126 and Camelyon17 following the previous methods. The SGD optimizer is used with learning rates adjusted to 0.01, 0.0001, 0.001 and 0.00005, respectively. The learning rate is proportionally decreased in the experiment studying the effect of batch size. The Kmeans Size is 512, Cluter Number is 4, Communication Interval is 10 across all the tasks. The perutrbaion magnitude α is fixed to 0.1 and the coefficient λ in loss function is fixed to 0.5. The δ parameter controlling the dependent sampling (Dirichlet distribution) is set to 0.1 for CIFAR10-C and adjusted to 0.01 for CIFAR100-C, ImageNet-C following UnMix-TNS [32]. Two threshold in Eq. 7 is set to the same value for corruption datasets and DomainNet126 following ETA [26]. While for Camelyon17, the class diversity related threshold is adjusted to 0.9 empirically.

B. Compared Methods

TBN [25] re-estimates batch normalization statistics from test data. TENT [34] minimizes prediction entropy to optimize batch normalization. CoTTA [36] addresses long-term test-time adaptation in changing environments. ETA [26] and SAR [27] exclude unreliable and redundant samples during optimization. AdaContrast [2] utilizes contrastive learning to refine pseudo-labels and improve feature learning. RoTTA [45] presents a robust batch normalization scheme with a memory bank for category-balanced estimation. RDumb [28] leverages weighted entropy and periodically resets the model to its pretrained state to prevent collapse. DeYO [17] quantifies the impact of object-destructive transformations for sample selection and weighting. UnMix-TNS [32] introduces a test-time normalization layer for non-i.i.d. environments by decomposing BN statistics. For fair comparisons, we conduct experi-

Table 5. Classification error rate (\downarrow) on CIFAR-10-C (C10), CIFAR-100-C (C100), and ImageNet-C (IN) using ResNet-50-BN & ViTBase-LN backbones under **Continual Setting**, averaged over 15 corruptions.

Methods	C10	C100	IN(BN)	IN(LN)
Source	43.5	46.5	82.0	60.2
TBN	20.4	35.4	68.6	-
TENT (ICLR 21')	20.0	62.2	62.6	54.5
ETA (ICML 22')	17.9	<u>32.2</u>	60.2	<u>49.8</u>
AdaContrast (CVPR 22')	18.5	33.5	65.5	57.0
CoTTA (CVPR 22')	16.5	32.8	63.1	77.0
SAR (ICLR 23')	20.4	32.0	61.9	51.7
RoTTA (CVPR 23')	19.3	34.8	67.3	58.3
RDumb (NeurIPS 23')	<u>17.8</u>	34.1	90.6	50.2
DeYO (ICLR 24')	87.0	98.1	90.6	94.3
UnMix-TNS (ICLR 24')	24.9	32.7	75.4	-
FreDA (ours)	19.5	32.5	60.2	47.9

ments using the open source online TTA repository [4]¹, which provides codes and configurations of state-of-the-art TTA methods.

C. Continual Setting Evaluation

Although our method is specifically designed for mixed domain scenarios, we also evaluated its performance under the conventional continual test-time adaptation setting to assess its robustness in different contexts. In this setting, the model adapts online to a sequence of test domains without explicit knowledge of domain shifts, with only one distribution shift occurring at a time and not reappearing. Without adjusting any parameters, our method demonstrated competitive performance compared to current state-of-the-art approaches. Notably, while UnMix-TNS effectively addresses non-i.i.d. issues (dependent sampling at the class level), it is less effective under i.i.d. conditions. Our results suggest that the proposed FreDA not only excels in its intended mixed domain scenarios but also generalizes effectively to standard continual adaptation tasks, providing a robust solution across various distributional challenges.

D. Parameter Study

In this section, we study the parameter choice of CLUSTER_NUM, KMEANS_SIZE and COMM_INTERVAL (refer to Algorithm 1 for detailed definitions). Results are reported in Table 6.

As we adjust the KMEANS_SIZE parameter from 256 to 2048, there is a remarkably consistent performance on

¹<https://github.com/mariodoebler/test-time-adaptation>

Table 6. Sensitivity analysis on different datasets.

CLUSTER_NUM	2	4	8	16
CIFAR10-C	23.0	22.9	23.2	24.7
CIFAR100-C	34.8	34.7	34.7	35.6
IN-C (BN)	68.6	67.2	67.1	70.5
IN-C (LN)	50.3	48.8	49.9	50.0
KMEANS_SIZE	256	512	1024	2048
CIFAR10-C	23.0	22.9	23.0	22.9
CIFAR100-C	34.6	34.7	34.8	34.8
IN-C (BN)	69.0	67.2	67.6	67.0
IN-C (LN)	49.0	48.8	48.7	48.8
COMM_INTERVAL	1	10	100	1000
CIFAR10-C	22.6	22.9	22.6	22.0
CIFAR100-C	34.7	34.7	34.9	43.2
IN-C (BN)	67.1	67.2	67.2	67.4
IN-C (LN)	48.4	48.8	48.8	48.7

different datasets, indicating that our method’s capability to generalize across various sizes.

The variation in CLUSTER_NUM across our datasets underscores the nuanced balance required in selecting the optimal branch number for domain adaptation. Utilizing just two clusters already yields relatively good results, suggesting that a minimal decentralization can be effective. However, as the number of clusters increases from 2 to 16, we observe a decline in performance on CIFAR100-C and a more pronounced deterioration on ImageNet-C, with the optimal performance achieved at a CLUSTER_NUM of 4. This trend underscores the delicate trade-off between model complexity and the risk of overfitting: employing too large a cluster size can lead to a model overly tailored to the training data, impairing its generalization capabilities.

For the sensitivity analysis of COMM.INTERVAL, we observe that our method is generally robust to changes in the communication interval across all datasets. However, the impact of communication frequency varies significantly among different datasets. For simpler datasets like CIFAR10, minimal communication, exemplified by an interval of $f = 1000$, yields the best results. This could be attributed to the model’s high accuracy, enabling positive feedback loops even within isolated branches. Conversely, for more complex datasets, more frequent communication, with intervals as low as $f = 1$, appears beneficial. This frequent updating may help prevent model degradation over time, especially in scenarios where the data complexity could lead to significant divergences in learning pathways among distributed model components.

E. Adaptation Scenarios

Mixed Domains: In this scenario, the model processes a long sequence of test samples where each sample $x_i \sim p_{s_i}(x)$ is independently drawn from a randomly selected target domain $\mathcal{D}_{s_i} \in \{\mathcal{D}_{t_1}, \mathcal{D}_{t_2}, \dots, \mathcal{D}_{t_N}\}$ and a randomly

selected class c_i among classes $\{1, 2, \dots, C\}$. The sequence is represented as:

$$\{x_1^{\mathcal{D}_{s_1}, c_1}, x_2^{\mathcal{D}_{s_2}, c_2}, \dots, x_k^{\mathcal{D}_{s_k}, c_k}\},$$

where each target domain index $s_i \in \{1, 2, \dots, N\}$ and class number $c_i \in \{1, 2, \dots, C\}$ are independently and randomly selected for each sample x_i .

Mixed Domains & Dependent Sampling: This scenario, extending the mixed distribution framework, introduces time-correlated sequential data emergence from the same class, featuring both covariate and label shifts. While the domain indices s_i are independently and randomly selected for each sample as before, the class labels are correlated over sequences of variable lengths. Specifically, the samples tend to come from the same class for a variable number of consecutive samples before potentially switching to a different class. The sequence can be represented as:

$$\begin{aligned} & \underbrace{\{x_1^{\mathcal{D}_{s_1}, C_1}, \dots, x_{l_1}^{\mathcal{D}_{s_{l_1}}, C_1}\}}_{\text{Samples from class } C_1} \\ & \rightarrow \underbrace{\{x_{l_1+1}^{\mathcal{D}_{s_{l_1+1}}, C_2}, \dots, x_{l_1+l_2}^{\mathcal{D}_{s_{l_1+l_2}}, C_2}\}}_{\text{Samples from class } C_2} \\ & \rightarrow \dots \rightarrow \underbrace{\{x_{l_1+\dots+l_{M-1}+1}^{\mathcal{D}_{s_{l_1+\dots+l_{M-1}+1}}, C_M}, \dots, x_k^{\mathcal{D}_{s_k}, C_M}\}}_{\text{Samples from class } C_M} \rightarrow \dots \end{aligned}$$

where:

- $s_i \in \{t_1, t_2, \dots, t_N\}$ are independently and randomly selected target domain index.
- l_j refers to the size of the j -th data segment in the sequence where $j = 1, 2, \dots, M$.
- $C_j \in \{1, 2, \dots, C\}$ denotes the class of samples within the j -th data segment.

F. Dataset Visualization

To further illustrate the characteristics of the datasets used in our evaluation, we present visualizations of the data distribution across different corruption types (Fig. 4), natural domain shifts (Fig. 5), and medical centers (Fig. 6). These figures highlight the diverse challenges that our models face in each evaluation scenario, providing insight into the complexity of the test conditions.

G. Limitation and Future Work

While FreDA addresses a critical challenge in handling heterogeneous data streams, providing a solid pipeline for this issue, there are still avenues for further enhancement.

Our current aggregation approach, which averages models based on cluster counts, has been effective in solving

the problem at hand. However, exploring alternative strategies—such as weighting models by the divergence between clusters—might lead to incremental improvements. Additionally, refining the sample selection process from a original sample-level focus to a more granular patch-level could extend FreDA’s applicability to tasks such as segmentation, thereby further enhancing its versatility in real-world scenarios.

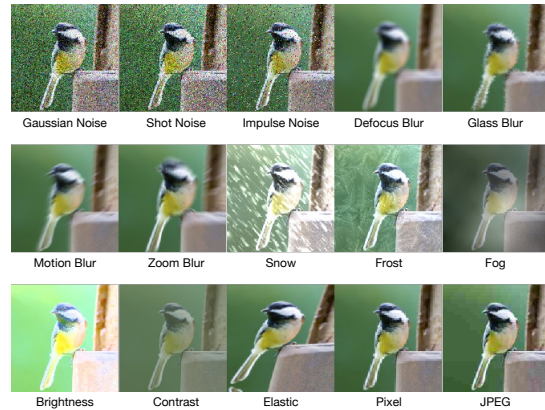


Figure 4. Examples from ImageNet-C under common image corruptions. The images showcase a range of corruption types (e.g., noise, blur, and weather distortions) at varying severity levels.

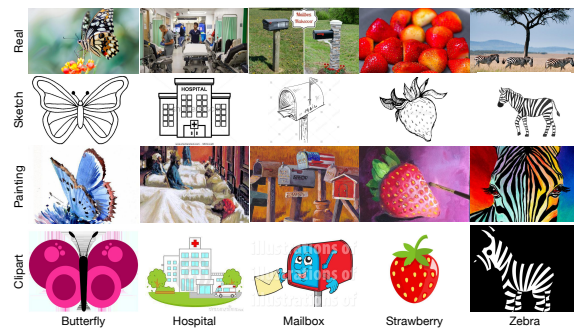


Figure 5. Samples from DomainNet126 across four subdomains (Real, Sketch, Painting, Clipart). These visualizations reflect the stylistic and perceptual variations inherent in each domain.

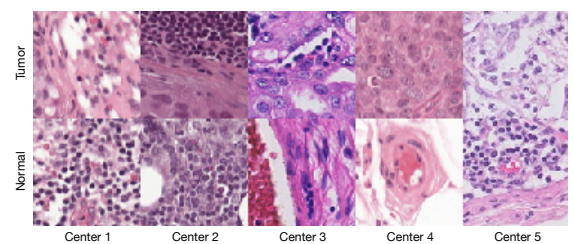


Figure 6. Example patches from the Camelyon17 dataset, containing histopathological images used for tumor detection.